UNIVERSITY OF
BATH

Citation for published version:
Lunt, AJG, Mohanty, G, Neo, TK, Michler, J & Korsunsky, AM 2015, Microscale resolution fracture toughness profiling at the zirconia-porcelain interface in dental prostheses. in S Palomba & BJ Eggleton (eds), Micro+Nano Materials, Devices, and Systems. vol. 9668, 96685S, SPIE, SPIE Micro+Nano Materials, Devices, and Applications Symposium, Sydney, Australia, 6/12/15. https://doi.org/10.1117/12.2199217

DOI:
10.1117/12.2199217

Publication date:
2015

Document Version
Peer reviewed version

Link to publication

University of Bath

Microscale resolution fracture toughness profiling at the zirconia- porcelain interface in dental prostheses

5 authors, including:

Alexander Lunt
University of Bath
43 PUBLICATIONS   **257** CITATIONS

SEE PROFILE

Gaurav Mohanty
Tampere University
32 PUBLICATIONS   **133** CITATIONS

SEE PROFILE

Johann Michler
Empa - Swiss Federal Laboratories for Materials Science and Technology
403 PUBLICATIONS   **6,697** CITATIONS

SEE PROFILE

Alexander M Korsunsky
University of Oxford
477 PUBLICATIONS   **5,255** CITATIONS

SEE PROFILE

Some of the authors of this publication are also working on these related projects:

Pushing the boundaries of Variable Temperature Nanomechanics View project

X-ray & Synchrotron studies View project

Microscale resolution fracture toughness profiling at the zirconia-porcelain interface in dental prostheses

Alexander J. G. Lunt*[a], Gaurav Mohanty[b], Tee K. Neo[c], Johann Michler[b] & Alexander M. Korsunsky[a]

[a] The Multi-Beam Laboratory for Engineering Microscopy, Department of Engineering Science, University of Oxford, Parks Road, Oxford, Oxfordshire, OX1 3PJ, United Kingdom.
[b] EMPA Materials Science & Technology, Thun, Feuerwerkerstrasse 39, CH-3602, Switzerland.
[c] Specialist Dental Group, Mount Elizabeth Orchard, 3 Mount Elizabeth, #08-03/08-08/08-10, Singapore 228510.

ABSTRACT

The high failure rate of the Yttria Partially Stabilized Zirconia (YPSZ)-porcelain interface in dental prostheses is influenced by the micro-scale mechanical property variation in this region. To improve the understanding of this behavior, micro-scale fracture toughness profiling by nanoindentation micropillar splitting is reported for the first time. Sixty 5 μm diameter micropillars were machined within the first 100 μm of the interface. Berkovich nanoindentation provided estimates of the bulk fracture toughness of YPSZ and porcelain that matched the literature values closely. However, the large included tip angle prevented precise alignment of indenter with the pillar center. Cube corner indentation was performed on the remainder of the pillars and calibration between nanoindentation using different tip shapes was used to determine the associated conversion factors. YPSZ micropillars failed by gradual crack propagation and bulk values persisted to within 15 μm from the interface, beyond which scatter increased and a 10% increase in fracture toughness was observed that may be associated with grain size variation at this location. Micropillars straddling the interface displayed preferential fracture within porcelain parallel to the interface at a location where nano-voiding has previously been observed. Pure porcelain micropillars exhibited highly brittle failure and a large reduction of fracture toughness (down to ~10%) within the first 50 μm of the interface. These new insights have the potential to facilitate improved micromechanical modelling of the interface region help in order to optimize current manufacturing routes and reduce failure.

Keywords: Fracture toughness, spatially resolved, yttria partially stabilized zirconia, porcelain, nanoindentation, micropillar splitting, microscale

1. INTRODUCTION

Yttria Partially Stabilized Zirconia (YPSZ) is a high strength, high toughness ceramic which in recent years has found increasing use in the manufacture of dental prostheses [1]. The origins of the toughening behavior of this material lie in the tetragonal to monoclinic YPSZ phase transformation which is induced at crack tips [2]. In dental applications YPSZ copings are veneered with porcelain in order to produce an aesthetically pleasing finish and to reduce the hardness of the outer surface, thereby reducing wear on existing opposing teeth [3]. However, this approach leads to the primary failure mode of YPSZ prostheses; near interface chipping of the porcelain veneer [4]. The origins of this failure are poorly understood but are believed to be linked to the mechanical property variation, residual stresses and porcelain creep induced in the near-interface region during prostheses manufacture [5-9].

Microanalysis and compositional mapping of the YPSZ-porcelain interface has been performed using a broad range of experimental techniques including Scanning Electron Microscopy (SEM) [10, 11], Energy Dispersive Spectroscopy (EDS) [11, 12], Transmission Electron Microscopy (TEM) [11, 13] and micro-beam diffraction [10, 14]. These studies have demonstrated that the microstructural variation of the YPSZ-porcelain is limited to within the first few hundred microns of the interface and that the behavior is influenced by both nano-voiding and nano-grain features. However these studies are not able to provide insight into the mechanical properties which are of most significance for integrity: stiffness,

*alexander.lunt@chch.ox.ac.uk; phone +441865 283447; www.korsunsky.org

hardness (yield strength) and toughness. Of these three, microscale spatially resolved studies of both Young's modulus and yield strength variation across the YPSZ-porcelain interface region have recently been published [11, 15, 16].

The knowledge of spatial variation of fracture toughness, or the material resistance to crack initiation and propagation, is critical in understanding the origins of the brittle failure observed at the YPSZ-porcelain interface. Quantification of the fracture toughness of both bulk YPSZ [17, 18] and bulk porcelain [19, 20] has been widely reported. However, no microscale spatially resolved analysis has been performed to determine the variation in the vicinity of the interface where failure is known to originate [21].

One of the most well-established and widely used procedures for microscale fracture toughness experimental determination is based on the measurement of the length of cracks induced by nanoindentation. It was first developed by Evans et al [22] in 1976. In recent years this approach has been refined to improve the resolution and precision of the technique, however this approach is highly sensitive to the shape of the crack, the exact shape of the indenter tip (due to manufacturing imperfections) and substrate mechanical properties [23]. Further, the impact of residual stress is known to influence greatly the crack propagation in this method, as demonstrated by a recent study by Sebastiani al [15] who used nanoindentation to quantify the average values of fracture toughness within 4 regions across a YPSZ-porcelain cross section, in which one average near-interface value for porcelain was reported. Since the magnitude of residual stress at the interface is known to be large and rapidly varying [16], de-convolution of this effect cannot be reliably performed for nanoindentation results at the microscale resolution required.

Recent improvements in nanoindentation systems and the increased availability of SEM-Focused Ion Beam (FIB) microscopes have facilitated the development of several new high resolution fracture toughness analysis techniques. A particular highly successful class of these methods is based around FIB milling and loading of notched micro-cantilevers [24-26]. Although these approaches benefit from high precision of crack positioning, there is currently disagreement in the literature over the sensitivity of the approach to the friction at the interface between the indenter surface (diamond) and the substrate, and the influence of ion beam damage at crack tips. The large FIB milling times associated with each measurement point also limits the applicability of this approach for spatially resolved study.

An alternative microscale fracture toughness approach based on Berkovich nanoindentation and fracture of micropillars has recently been published by Sebastiani et al. [23, 27]. This approach benefits from a well-defined microscale gauge volume, the complete relief of residual stress in the examined region prior to indentation that minimizes the impact of this effect on the result, and from fracture originating from a location unaffected by FIB milling. Additionally, the method can be implemented in a relatively short time frame, opening the possibilities of fracture toughness profiling and mapping. These benefits make it highly suitable for spatially resolved fracture toughness analysis across the YPSZ-porcelain interface.

2. METHODOLOGY

2.1 Sample preparation

An incisal YPSZ-porcelain dental prosthesis was manufactured by technicians at the DE Dental Lab, Singapore. The assembly process employed was identical to that used in commercial samples: a YPSZ prostheses coping was produced by shaping lightly pre-sintered Zenotec Zr Bridge [28] into the form required. This was then sintered at 1600°C to produce a fully dense component. Multiple layers of IPS e.max Ceram [29] were then applied to the surface of the coping in order to produce a realistic and aesthetically pleasing finish.

In order to gain access to the interface, the completed prosthesis was mounted in epoxy resin and a 2 mm thick cross sectional slice was obtained using Buehler Isomet Diamond Saw. An incremental grinding and polishing process was then used to remove any material influenced by the cutting process and to minimize the magnitude of residual stresses induced by sample preparation. The sample was then mounted on an SEM stub using silver paint in order to provide an effective conduction path and thereby minimize charging during FIB milling and SEM imaging.

2.2 Micropillar FIB machining

FIB milling was used to generate an array of micropillars which were aligned in a direction perpendicular to the interface as shown in Figure 1a. This pattern was selected to maximize the number of pillars within the first 15 μm of the interface in order to enable improved statistics to be captured in the location where most variation was expected. FIB milling was performed on the TESCAN Lyra 3 FIB-SEM at the Multi-Beam Laboratory for Engineering Microscopy (MBLEM),

Oxford, UK using an automated script for pillar milling, and a milling current of 1.25 nA. A nominal pillar diameter and depth of 5 μm was selected in order to provide the required resolution while simultaneously minimizing the impact of ion beam damage on the fracture toughness recorded. This size was also consistent with the successful experiments previously performed by Sebastiani et al [27]. A trench width of 3 μm was selected as a compromise between maximizing the spatial resolution of the data collected and ensuring that there was no interaction between the indenter and the surrounding material. In order to aid in aligning the indenter on the center of each pillar a 25 nm deep cross was milled into the surface as shown in Figure 1b. High resolution imaging was performed on each pillar in using SEM stage tilt angles of 0° and 35° in order to measure the radius (R) and height of each pillar using the technique previously outlined by Lunt et al. [11]. Precise measurement of the distance from the interface to the center of each pillar was also performed during this process.
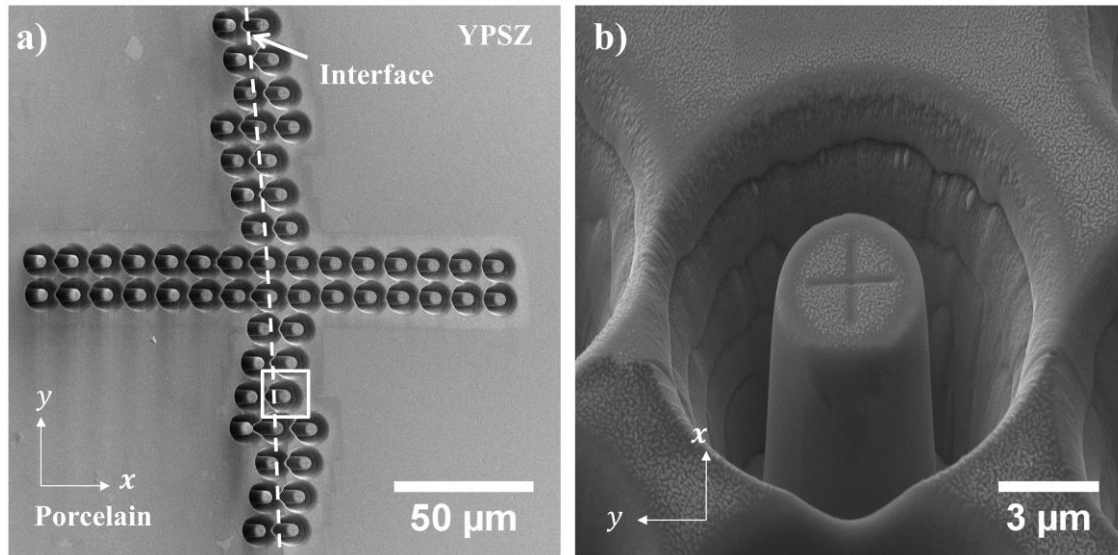

Figure 1. a) Positions of FIB milled micropillars across the YPSZ-Porcelain interface. The number of pillars near to the interface has been chosen to be large in order to gain improved insight into the statistics of this region. b) A high magnification of one of the pillars (the location of which is shown in Figure 1a showing the indentation alignment cross on the center of the pillar. Both images were captured at a SEM tilt of 55° using tilt correction in the x direction. Figure 1a has been rotated to be orientationally consistent with the other figures presented in this study.

2.3 Micropillar indentation splitting

Micropillar indentation splitting was performed using an Alemnis SEM Indenter inside the TESCAN Lyra 3 FIB-SEM at Empa, Thun, Switzerland. Prior to the start of the experiment, compliance calibration was performed by indenting fused silica which has a well characterized indentation response. Before each indentation, the tip was cleaned by indenting the polymer substrate in which the prosthesis was embedded. A displacement control mode was used during the analysis in order to prevent the large displacements typically observed during fracture under load control. The purpose of this approach is to enable the failure mode of the pillars to be examined in more detail through SEM imaging of the fractured pillars. Videos of the indentation were also recorded to provide further insight into the pillar failure behavior as shown in Videos 1a and 1b (see supplementary information).

Preliminary micropillar indentation splitting was performed using the approach pioneered by Sebastiani et al. [27]. A diamond Berkovich tip, with a total included angle of $142.3°$ was used to perform this analysis. This facilitated the use of the Berkovich indentation load pre-multiplier (γ_B) values which have previously been published for this technique. The relationship between the Berkovich fracture toughness (K_B), critical failure load (P_C) and pillar radius (R) is then given by:

$$K_B = \gamma_B \frac{P_C}{R^{3/2}}.$$

(1)

The large included angle associated with this indenter type is known to reduce the sliding between the indenter and pillar surfaces. This ensures that the fracture load is less dependent upon the frictional coefficient between these two surfaces (a parameter which is typically unknown). In spite of this, the shallow viewing angle imposed by the tip presents difficulties in aligning the indenter tip to the center of the pillar. The SEM imaging performed is constrained by the geometry of the indenter and thereby reduces the precision with which this can be performed along the direction of the beam. In total 9 indents were performed in the YPSZ using this approach and 3 indents were performed in porcelain, taking an average time of 40 minutes per point. All of these points were selected to be far from the interface where the variation in fracture toughness was expected to be small.
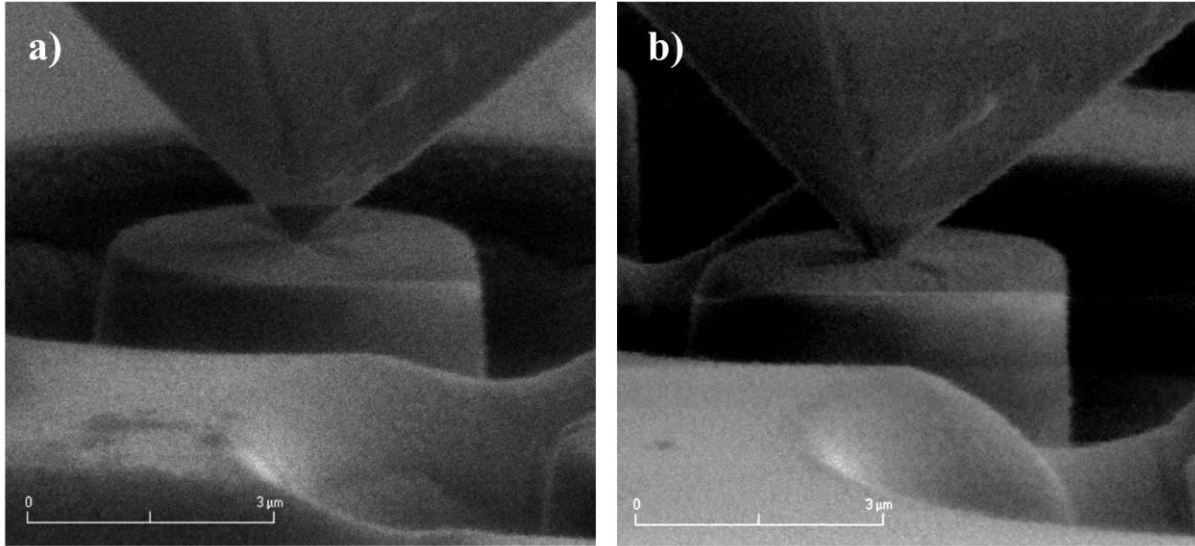
Video 1a and 1b. Videos of cube corner nanoindentation splitting in a) YPSZ (9 µm from interface) and b) porcelain (11 µm from interface). The more ductile fracture mode of YPSZ and brittle response of porcelain are demonstrated in these two videos. http://dx.doi.org/doi.number.goes.here

In order to increase the precision of the alignment between the indenter tip and the center of the pillar and reduce the time required to indent the remaining 48 pillars, the decision was made to change to a diamond cube corner indenter tip. The reduced included angle of 90° associated with this tip geometry increases the sensitivity of the technique to the friction between diamond and the substrate material and means that the value of γ_B previously published by Sebastiani et al. [27] is no longer valid. Despite this, direct comparison between the fracture toughness results obtained using Berkovich and cube corner indentation tips can be used to provide an estimate of the cube corner indentation load pre-multiplier (γ_C) for a given material as outlined in Section 3.2. Indentation was then performed on all of the remaining pillars in an average time of 11 minutes per point. Imaging of the fractured pillars was implemented using the Hitachi S-4800 (CFE) SEM at EMPA, Thun, Switzerland with an imaging direction which was normal to the surface of the substrate.

3. RESULTS

3.1 Young's modulus and hardness variation at the YPSZ-porcelain interface

In order to perform fracture toughness evaluation through micropillar splitting, insight into the Young's modulus (E) and hardness (H) within the region of interest is required. The ratio between these parameters can then be used to calculate the load pre-multiplier γ_B through Finite Element (FE) simulations. A plot of the relationship between E/H and γ_B was recently published by Sebastiani et al [23] which demonstrates that for E/H values ranging from 5 to 22 this relationship is approximately linear and can be fitted to give the following relationship:

$$\gamma_B = 0.0149\frac{E}{H} + 0.057. \tag{2}$$

The spatial distribution of Young's modulus and yield strength (or fracture strength) across the interface of an identical YPSZ-porcelain dental prosthesis was recently published in a micropillar compression by Lunt et al. [11]. The quantitative

values obtained using this approach are known to be independent of the high magnitude residual stresses in the near-interface region due to the full stress relaxation induced in the pillars prior to compression. Consequently the Young's modulus identified during this analysis were found to be close to the published values published; for YPSZ this estimate was 216 GPa compared to 210 GPa provided by the manufacturer [28] and for porcelain this estimate was 70 GPa compared to the bulk value of 60 GPa previously reported in the literature [30].

Although nanoindentation has previously been successfully performed across the YPSZ-porcelain interface [15, 16], the influence of residual stress and brittle fracture (inelastic behavior) is known to influence hardness measurements obtained in these types of system [31]. However, in order to gain insight into the likely trends in hardness across the interface, the approximately constant relationship that exists between yield strength (σ_y) and hardness for a given material can be exploited. Although the exact relationship between these two parameters is highly dependent upon the specific substrate, a good approximation for the relationship is that hardness is three times the yield strength [32]. Comparison between the average yield strength obtained through microcompression [11] and those provided in the literature, demonstrate that this is a good approximation for YPSZ (13.5 GPa compared to 12.75 GPa provided by the manufacturer [28]) but not for porcelain (10.3 GPa compared to 5.4 GPa published in the literature [33]). These differences are likely associated with size effects and the differing microstructures of the two materials.

Therefore, in order to provide insight into the likely variation of the ratio between Young's modulus and hardness across the YPSZ – porcelain interface, the results obtained by micropillar compression [11] were used in the following approximation:

$$\frac{E(x)}{H(x)} \approx \frac{E(x)}{3\sigma_y(x)},$$

(3)

where x is the distance from the interface. The standard deviations of E and σ_y were used to calculated the 95% confidence intervals of E/H and the results are shown in Figure 2.
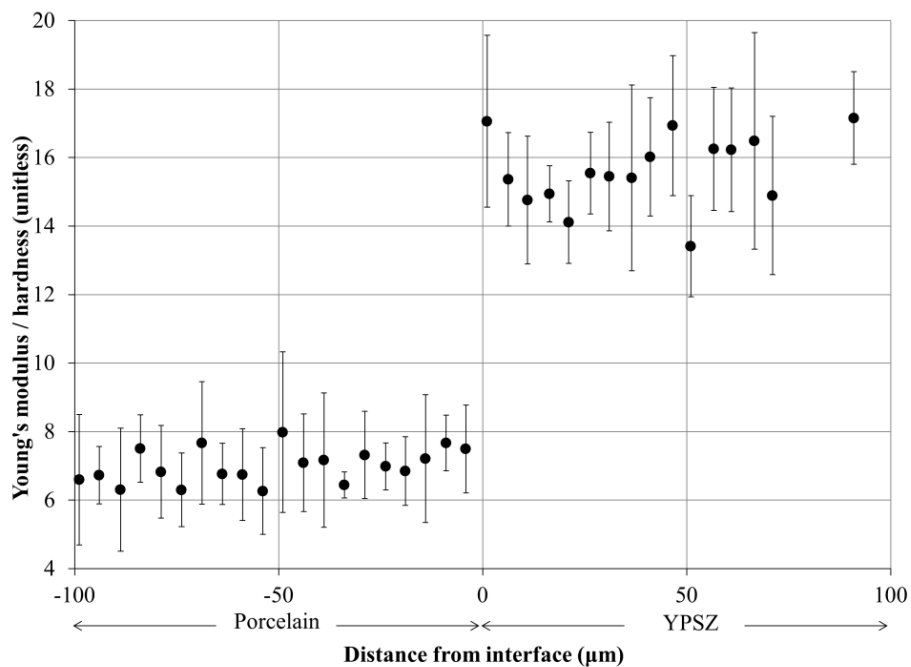

Figure 2. Variation of Young's modulus / hardness as a function of distance from the YPSZ-porcelain interface. The data values obtained for this distribution were taken from micropillar compression study published by Lunt et al. [11] and have made use of the approximation that hardness is approximately equal to 3 times the yield strength. The error bars indicate the 95% confidence intervals of each value.

Critical examination of Figure 2 reveals that within each material the scatter of E/H is generally equal to or smaller than the 95% confidence intervals of each value. This means that, to within the scatter of the results obtained experimentally, the value of E/H can be considered to be approximately constant in both YPSZ and porcelain. Further, as highlighted in Equation 2, it can be seen that moderate changes in the value of E/H result in very small changes in γ_B, i.e. the fracture toughness estimate is robust to minor deviations in E/H. This approximation of constant material mechanical parameters in both YPSZ and porcelain was therefore used in the remainder of the analysis.

It was decided that the literature values of Young's modulus and hardness would be used to calculate the E/H ratio for both YPSZ and porcelain as shown in Table 1. The magnitude of these bulk estimates are typically more reliable than the results of micro-mechanical testing and the use of these values is also consistent with the approach implemented by Sebastiani et al. [27].

Table 1. Mechanical properties indentation load pre-multipliers for YPSZ and porcelain. Literature values of Young's Modulus (E), hardness (H) and fracture toughness (K) are given with references, along with the calculated values of the Berkovich and cube corner indentation load pre-multipliers (γ_B and γ_C, respectively). The average fracture toughness estimate obtained from Berkovich indentation (K_B) is included for comparison. The standard deviation of each measurement has been included in the table where values are known.

Material	E (GPa)	H (GPa)	K (MPam$^{0.5}$)	γ_B	γ_C	K_B (MPam$^{0.5}$)
YPSZ	210 [28]	12.75 $\pm$ 1.96 [28]	5.00 [28]	0.31 $\pm$ 0.02	1.10 $\pm$ 0.05	4.79 $\pm$ 0.24
Porcelain	60 [34]	5.40 $\pm$ 0.20 [33]	2.75 $\pm$ 0.25 [33]	0.22 $\pm$ 0.01	0.41 $\pm$ 0.04	2.65 $\pm$ 0.27

3.2 Micropillar indentation splitting

After successfully fracturing each of the 60 FIB milled pillars, analysis was performed on the load-displacement curves obtained from the analysis. Distinct differences were observed between the fracture of the YPSZ and porcelain micropillars, examples of which are shown in Figure 3. In the case of porcelain, brittle failure occurred without the onset of plasticity. However in the case of YPSZ, a gradient decrease in the load-displacement plot was observed prior to failure. Despite these differences consistent estimates of the critical instability load (P_C) were obtained from each of the pillars from the point where large drops were observed in the load.
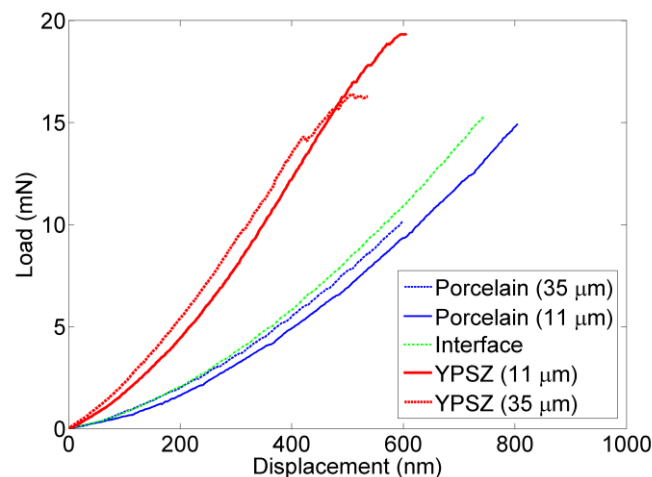

Figure 3. Typical load-displacement plots for YPSZ, porcelain and the interface up to the point of brittle failure. The distance from the interface to the pillar center is given in the plot legend. YPSZ shows plasticity prior to critical failure whereas no reduction in gradient is observed in porcelain or the interface indentation.

In order to obtain estimates of the fracture toughness of each of the pillars, quantification of the Berkovich indentation load pre-multiplier γ_B for each material were next obtained. These were based on the bulk values of Young's modulus and hardness for YPSZ and porcelain outlined in Table 1 and Equation 2 [23]. Estimates of the Berkovich fracture toughness

were then obtained using Equation 1. In order to provide comparisons with the cube corner indentations, the average value of K_B was determined at positions at which both techniques had been applied; at $60, 70$ and $80 \mu m$ from the interface for porcelain and at $35, 50$ and $60 \mu m$ from the interface for YPSZ. The averages and standard deviations of K_B obtained from these three points are given in Table 1. These estimates were then treated as absolute measures of fracture toughness in order to optimize γ_C, the cube corner indentation load pre-multiplier for each material. This parameter relates the cube corner fracture toughness K_C to the critical instability load, through the expression:

$$K_C = \gamma_C \frac{P_C}{R^{3/2}}. \tag{4}$$

The magnitude and standard deviation of γ_C for YPSZ and porcelain obtained from this analysis are given in Table 1. These estimates were then used in combination with the critical fracture toughness values to obtain estimates of the K_C in the YPSZ and porcelain near-interface regions. At the locations where both YPSZ and porcelain were contained within the pillar an average value of $\gamma_C = 0.5 \times \left(\gamma_C^{Zir} + \gamma_C^{Por} \right)$ was used to determine K_C. The standard deviations of the fracture toughness values were obtained from the combined uncertainties of each of the parameters used in their calculation and the results of this analysis are shown in Figure 4.
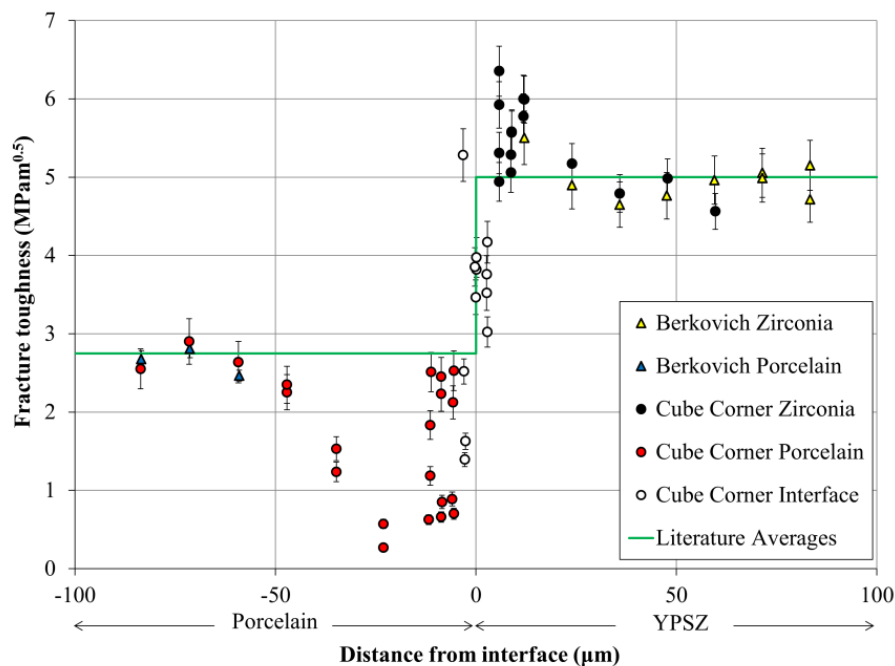

Figure 4. Fracture toughness variation across the YPSZ – porcelain interface showing YPSZ on the right (positive distances) and porcelain on the left (negative distances). The results from both Berkovich and cube corner indentation are shown along with the average values obtained from the literature [28, 33]. At the interface an average of the γ values for the two materials was used to calculate the fracture toughness. The error bars shown indicate the 95% confidence intervals of each measurement.

Examination of the SEM images of the fractured pillars revealed that the average offset between the center of the pillar and the indenter tip was less than 100 nm for the cube corner indentations, compared with $100 - 300 \, nm$ for the Berkovich tip. Four main failure modes were observed in the pillars depending upon the substrate material, location and indenter tip geometry as shown in Figure 5. Examination of the porcelain micropillars revealed that for many of the tested positions, the indentation had been sufficient to fully fracture the stub, leaving only the base or a small section of the pillar (Figure 5a). The smooth, sharp facets observed on the remaining surfaces suggested that porcelain failure was brittle, in contrast to the gradual failure observed in YPSZ. In near-interface pillars, which contained both YPSZ and porcelain within a single pillar (Figure 5b), a different failure mode was widely observed. Typically the pillar was found to fracture into two pieces, with the direction of fracture being closely aligned to the interface direction. The fracture observed in these pillars was sharp suggesting a single failure event, and the crack was typically induced within the porcelain at a distance

Author Accepted Manuscript – This work was presented at SPIE Micro+ Nano Materials, Devices and Applications – Sydney, Australia – December 2015

Final published version can be found at doi:10.1117/12.2199217

of between $1 - 2$ μm from the interface. Cube corner indentation of YPSZ resulted in pillar splitting along the sharp edges of the indent as shown in Figure 5c. The surface of these fractures was highly faceted suggesting failure did not propagate fully during a single fracture event, but increased gradually through the continued application of load. In contrast to this behavior, Berkovich indentation cracks were localized to pillar edges in YPSZ, this was believed to be associated sub-surface cracking which propagated to the pillar surface as shown in Figure 5d.
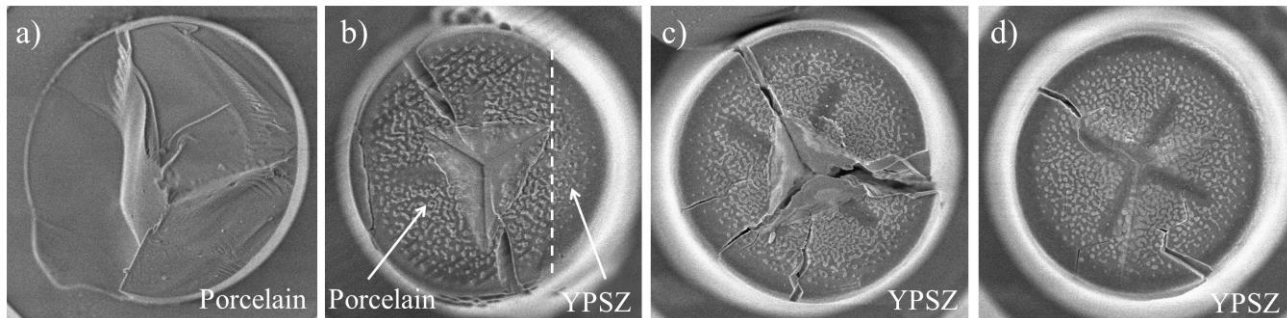

Figure 5. SEM images of fractured pillars. a) Complete brittle failure of the porcelain micropillar located 47 μm from the interface. The remaining stub base is shown, along with the smooth fracture surfaces. b) Typical near-interface cube corner micropillar failure showing the pillar splitting into two halves. Examination of multiple interface fractures revealed that the fracture direction was often closely aligned to the interface. c) Typical YPSZ cube corner tip fracture showing multiple cracks from the center to the edge of a pillar located 11 μm from the interface. d) Berkovich tip indentation of the YPSZ micropillar located at 35 μm from the interface. Two cracks can be observed from the edge of the pillar running towards the center.

4. DISCUSSION

Examination of the fracture toughness variation across the interface in Figure 4 reveals that beyond 50 μm from the interface in porcelain and beyond 25 μm in YPSZ, the fracture toughness is approximately constant and equal to the average values published in the literature [28, 33]. This suggests that the results obtained though the of Berkovich pillar splitting approach developed by Sebastiani et al [23, 27] are reliable in both YPSZ and porcelain. Further, the minimal variation in fracture toughness ensures that the calibration of γ_C implemented based on constant K values outlined in Section 3.2 is valid.

The values of γ_C for YPSZ and porcelain were determined to be 1.10 and 0.41 respectively. Pillar splitting using a cube corner indentation tip has not previously been published in the literature and therefore no comparative results are available The magnitude of these pre-multipliers are several times larger than the equivalent γ_B values for each material and are known to be associated with the sharper indentation and increased surface sliding associated with a cube corner indent.. This induces a different type of pillar failure as highlighted in Figures 5a and 5b but also increases the sensitivity of the technique to the friction coefficient between the diamond tip and the substrate material. Despite these differences, the variation in fracture toughness obtained through cube corner indentation appears to be realistic and can begin to explain some of the failures observed in this system.

In order to gain insight into the scatter observed within the very near interface region (< 15 μm) a systematic examination was performed to assess factors which may have influenced these values. No correlation could be observed between the fracture toughness and the magnitude of misalignment between the pillar center and the indentation position. In contrast, the analysis instead revealed that the pillar splitting approach is robust to minor errors in indenter positioning. Analysis was also performed to assess the impact of spatial positioning (along the interface direction), pillar diameter and pillar height on the fracture toughness values obtained. No trends could be identified in any of these parameters, suggesting that the scatter observed in the near-interface region is instead more likely to be representative of the random fracture toughness variation at this location.

As previously highlighted in Section 3.2, distinct differences were observed between the YPSZ, porcelain and interface (containing both YPSZ and porcelain) failure modes. Video 1a and Figure 3 both demonstrate that the failure of YPSZ is gradual and occurs by crack propagation and slow growth under increasing load. This results in a reduction in gradient on the load-displacement curve which is indicative of energy absorption and a 'plastic' type failure. The multi-faceted crack

Author Accepted Manuscript – This work was presented at SPIE Micro+ Nano Materials, Devices and Applications –
Sydney, Australia – December 2015

Final published version can be found at doi:10.1117/12.2199217

surfaces observed in the fractured pillars (Figure 5c) provide further evidence that YPSZ failure is associated with gradual crack growth. In contrast to this behavior, Video 1b and Figure 3 highlight the brittle failure mode induced in porcelain. There is no change in gradient on the load-displacement curve and complete pillar fracture occurs at a point at which there were no visible cracks in the pillar surface.

In the near interface region, a distinct failure mode is observed which is believed to be a combination of both the YPSZ and porcelain failure mechanisms and preferential pillar splitting along the direction of the YPSZ-porcelain interface. Planar interfaces are implicitly associated with orientational dependence and therefore it is perhaps unsurprising that the half pillar splitting observed in the interface region is preferentially aligned to the interface. What is however more surprising is that failure was not observed at the interface location, where a step change in mechanical properties is expected, or at the pillar center. Failure was found to be more likely within the near-interface porcelain at a distance of between $1 - 2$ μm from the interface. This length scale correlates well with the position of nanoscale voiding observed in porcelain by Lunt et al. [11] ($0.4 - 1.5$ μm from the interface) suggesting that there may be an implicit weakness in the porcelain at this location. The random nature of void type features may also explain the large scatter observed in the fracture toughness of the near-interface porcelain pillars.

Clear differences can be observed between the literature average values of fracture toughness and those obtained micropillar splitting for both YPSZ and porcelain in the near-interface region (Figure 4). A clear reduction in fracture toughness (by up to ~90%) is observed in porcelain starting at a distance of approximately 50 μm from the interface and extending to the near interface location. This variation is highly self-consistent in the pillars between 50 and 15 μm from the interface, suggesting that this weakness may be associated with a gradual variation in mechanical properties. For example, elemental diffusion or long-range grain refinement effects, both of which are known to influence the fracture toughness behavior of porcelain [35]. In contrast to this behavior, at distances less than 15 μm from the interface, a large amount of scatter is observed within the data suggesting more statistically driven weaknesses than those observed at larger distances. The fracture toughness estimates within this range vary from $0.6 - 2.5$ MPam$^{0.5}$ which demonstrates that the bulk mechanical behavior is present within some near-interface positions.

The variation of fracture toughness within the interface pillars (containing both YPSZ and porcelain) demonstrates relatively high levels of scatter with an average value of 3.8 MPam$^{0.5}$. This corresponds well with the average literature fracture toughness values of YPSZ and porcelain of 3.9 MPam$^{0.5}$. Despite this consistency, the fracture toughness in pillars containing mostly porcelain shows high levels of scatter. Of the four pillars measured, three are within the scatter observed in the neighboring porcelain however one high toughness pillar (5.3 MPam$^{0.5}$) was observed at this location, this may be an outlier or perhaps is more representative of failure within YPSZ.

In YPSZ the fracture toughness is approximately constant and equal to the literature value of 5 MPam$^{0.5}$ up a distance of 15 μm from the interface. In the near-interface region, an increase in fracture toughness is observed up to an average value of 5.5 MPam$^{0.5}$. An increase in scatter is also observed in this region with values between $4.9 - 6.4$ MPam$^{0.5}$ being observed. This again suggests that this behavioral change is statistically driven, rather than a gradual transition and therefore is likely to be associated with local features. At present the exact origin of this increased toughness is not clear. One explanation may be high elemental composition sensitivity of YPSZ fracture toughness [18, 36] and the variations in the concentration of Si, K, Na and Al known to be present within the first 5 μm of the interface [11]. Perhaps more likely, given the scatter in the fracture toughness values obtained, is the grain size dependence of YPSZ fracture toughness [37]. Larger grains of YPSZ are more likely to transform from a tetragonal to a monoclinic phase during stress application, increasing the amount of energy absorbed by the material during fracture. TEM of the YPSZ-porcelain interface has previously highlighted YPSZ grain size variations at this location, including the presence of relatively large grains ($1 - 2$ μm^2) within the first 10 μm of the interface [11]. The scatter observed may therefore be dependent upon the presence, or lack of, a large grain within the gauge volume under consideration.

5. CONCLUSIONS

This study is the first published work which outlined the application of spatially resolved fracture toughness using nanoindentation and pillar splitting. The approach has been shown to provide reliable estimates of fracture toughness in the ceramics YPSZ and porcelain and has been used to investigate the variation of fracture toughness within a sample of commercial interest; the YPSZ-porcelain interface in dental prostheses. Further, cube corner indentation (which can be aligned more quickly and precisely to pillar centers) has been shown to provide realistic estimates of fracture toughness

Author Accepted Manuscript – This work was presented at SPIE Micro+ Nano Materials, Devices and Applications – Sydney, Australia – December 2015

Final published version can be found at doi:10.1117/12.2199217

by making use of the critical failure load pre-multiplier γ_C. Estimates of γ_C for both YPSZ and porcelain were obtained by comparison with the Berkovich indentation approach previously published by Sebastiani et al. [23, 27].

Near interface YPSZ has been shown to fail through a gradual, 'plastic' type fracture mode and has shown to be consistent with literature estimates of fracture toughness at distances beyond 15 μm from the interface. In the very near interface region, a 10% increase in fracture toughness was observed, along with an increase in scatter. This may be associated with grain size variation and the associated impact on fracture toughness in YPSZ.

In pillars which contained both YPSZ and porcelain, a distinctive half pillar splitting type failure was observed which was typically aligned with the interface and was positioned in the porcelain at a distance of $1 - 2$ μm from the interface. This behavior is believed to be associated with the nanoscale voiding previously observed in porcelain at this location.

Porcelain micropillar failure was found to be brittle in nature, with no plasticity or cracking observed before complete failure of the micropillar. Scatter was observed within the very near-interface (< 15 μm) fracture toughness values suggesting a statistically driven failure which was dependent upon local features. Further variation in fracture toughness was observed up to 50 μm from the interface which demonstrated a gradual and consistent reduction in toughness (of up to $\sim 90\%$). This large reduction in fracture toughness, in combination with the high magnitude residual stresses at this location, has the potential to explain the high failure rates observed in this micromechanical system.

The insights gained by this study can be used in combination with other recent high resolution mechanical studies of the YPSZ-porcelain interface in order to develop improved models of the evolution of residual stress, microstructure and mechanical behavior. These simulations can be used to optimize the thermal processing routes applied during manufacture in order to reduce the impact of localized residual stress and fracture toughness variation, with the ultimate goal of reducing prosthesis failure rates.

ACKNOWLEDGMENTS

REFERENCES

[1]   I. Denry, and J. R. Kelly, "State of the art of zirconia for dental applications," Dental Materials, 24(3), 299-307 (2008).

[2]   B. Basu, "Toughening of yttria-stabilised tetragonal zirconia ceramics," International Materials Reviews, 50(4), 239-256 (2005).

[3]   R. Hmaidouch, and P. Weigl, "Tooth wear against ceramic crowns in posterior region: a systematic literature review," International journal of oral science, 5(4), 183-190 (2013).

[4]   N. R. F. A. Silva, E. A. Bonfante, R. A. Zavanelli et al., "Reliability of Metalloceramic and Zirconia-based Ceramic Crowns," Journal of dental research, 89(10), 1051-1056 (2010).

[5]   M. Baldassarri, C. F. J. Stappert, M. S. Wolff et al., "Residual stresses in porcelain-veneered zirconia prostheses," Dental Materials, 28(8), 873-879 (2012).

[6]   R. Belli, R. Frankenberger, A. Appelt et al., "Thermal-induced residual stresses affect the lifetime of zirconia–veneer crowns," Dental Materials, 29(2), 181-190 (2013).

[7]   B. Al-Amleh, J. N. Waddell, K. Lyons et al., "Influence of veneering porcelain thickness and cooling rate on residual stresses in zirconia molar crowns," Dental Materials, 30(3), 271-280 (2014).

[8]   A. J. G. Lunt, S. Kabra, J. Kelleher et al., "Tensile Secondary Creep Rate Analysis of a Dental Veneering Porcelain," Thin Solid Films, In Press - Corrected Proof, (2015).

[9]   A. J. G. Lunt, T. K. Neo, and A. M. Korsunsky, "An Electron Microscopy Study of Sintering in Three Dental Porcelains," Proc WCE, 2, (2015).

[10]   D. Liu, J. P. Matinlinna, J. K.-H. Tsoi et al., "A new modified laser pretreatment for porcelain zirconia bonding," Dental Materials, 29(5), 559-565 (2013).

[11]   A. J. G. Lunt, G. Mohanty, S. Ying *et al.*, "A Comparative Transmission Electron Microscopy, Energy Dispersive X-ray Spectroscopy and Spatially Resolved Micropillar Compression Study of the Yttria Partially Stabilised Zirconia–Porcelain Interface in Dental Prosthesis," Thin Solid Films*,* In Press - Corrected Proof, (2015).

[12]   Y. Kawai, M. Uo, and F. Watari, "Microstructure evaluation of the interface between dental zirconia ceramics and veneering porcelain," Nano Biomedicine*,* 2(1), 31-36 (2010).

[13]   A. Grigore, S. Spallek, A. Petschelt *et al.*, "Microstructure of veneered zirconia after surface treatments: A TEM study," Dental Materials*,* 29(11), 1098-1107 (2013).

[14]   T. F. Alghazzawi, and G. M. Janowski, "Evaluation of zirconia–porcelain interface using X-ray diffraction," International journal of oral science*,* 7(3), 187-195 (2015).

[15]   M. Sebastiani, F. Massimi, G. Merlati *et al.*, "Residual micro-stress distributions in heat-pressed ceramic on zirconia and porcelain-fused to metal systems: Analysis by FIB–DIC ring-core method and correlation with fracture toughness," Dental Materials, (2015).

[16]   Y. Zhang, M. Allahkarami, and J. Hanan, "Measuring residual stress in ceramic zirconia–porcelain dental crowns by nanoindentation," J Mech Behav Biomed Mater*,* 6, 120-127 (2012).

[17]   A. Selçuk, and A. Atkinson, "Strength and Toughness of Tape-Cast Yttria-Stabilized Zirconia," Journal of the American Ceramic Society*,* 83(8), 2029-2035 (2000).

[18]   K. Tsukuma, K. Ueda, and M. Shimada, "Strength and Fracture Toughness of Isostatically Hot-Pressed Composites of Al2O3 and Y2O3-Partially-Stabilized ZrO2," Journal of the American Ceramic Society*,* 68(1), C-4-C-5 (1985).

[19]   R. Morena, P. Lockwood, and C. Fairhurst, "Fracture toughness of commercial dental porcelains," Dental Materials*,* 2(2), 58-62 (1986).

[20]   S. Scherrer, J. R. Kelly, G. D. Quinn *et al.*, "Fracture toughness (K IC) of a dental porcelain determined by fractographic analysis," Dental Materials*,* 15(5), 342-348 (1999).

[21]   M. Guazzato, K. Proos, L. Quach *et al.*, "Strength, reliability and mode of fracture of bilayered porcelain/zirconia (Y-TZP) dental ceramics," Biomaterials*,* 25(20), 5045-5052 (2004).

[22]   A. G. Evans, and E. A. Charles, "Fracture toughness determinations by indentation," Journal of the American Ceramic Society*,* 59(7-8), 371-372 (1976).

[23]   M. Sebastiani, K. Johanns, E. Herbert *et al.*, "Measurement of fracture toughness by nanoindentation methods: Recent advances and future challenges," Current Opinion in Solid State and Materials Science, (2015).

[24]   D. Di Maio, and S. Roberts, "Measuring fracture toughness of coatings using focused-ion-beam-machined microbeams," J Mater Res*,* 20(02), 299-302 (2005).

[25]   A. Riedl, R. Daniel, M. Stefenelli *et al.*, "A novel approach for determining fracture toughness of hard coatings on the micrometer scale," Scripta Materialia*,* 67(7–8), 708-711 (2012).

[26]   S. Liu, J. M. Wheeler, P. R. Howie *et al.*, "Measuring the fracture resistance of hard coatings," Applied Physics Letters*,* 102(17), 171907 (2013).

[27]   M. Sebastiani, K. Johanns, E. Herbert *et al.*, "A novel pillar indentation splitting test for measuring fracture toughness of thin ceramic coatings," Philosophical Magazine((ahead of print)), 1-17 (2014).

[28]   "Zenotec Zr Bridge," http://www.wieland-dental.de/en/products/zenotec/materials/zenotec-zr-bridge/ (10/09/15).

[29]   "IPS e.max Ceram," http://www.ivoclarvivadent.co.uk/en/products/all-ceramics/ips-emax-technicians/ips-emax-ceram (19/02/15).

[30]   M. Uchic, P. Shade, and D. Dimiduk, "Micro-compression testing of fcc metals: A selected overview of experiments and simulations," JOM-J Min Met Mat S*,* 61(3), 36-41 (2009).

[31]   W. C. Oliver, and G. M. Pharr, "An improved technique for determining hardness and elastic modulus using load and displacement sensing indentation experiments," Journal of Materials Research*,* 7(06), 1564-1583 (1992).

[32]   P. Zhang, S. X. Li, and Z. F. Zhang, "General relationship between strength and hardness," Materials Science and Engineering: A*,* 529, 62-73 (2011).

[33]   "IPS e.max® Ceram Scientific Documentation," www.roedentallab.com/downloads/emaxceramicdata.pdf (19/02/15).

[34]   M. D. Uchic, and D. M. Dimiduk, "A methodology to investigate size scale effects in crystalline plasticity using uniaxial compression testing," Mater Sci Eng A*,* 400(0), 268-278 (2005).

[35]   J. Quinn, V. Sundar, and I. Lloyd, "Influence of microstructure and chemistry on the fracture toughness of dental ceramics," Dental Materials*,* 19(7), 603-611 (2003).

[36]   O. Vasylkiv, Y. Sakka, and V. V. Skorokhod, "Hardness and fracture toughness of alumina-doped tetragonal
        zirconia with different yttria contents," Materials Transactions, 44(10), 2235-2238 (2003).
[37]   M. Trunec, and Z. Chlup, "Higher fracture toughness of tetragonal zirconia ceramics through nanocrystalline
        structure," Scripta Materialia, 61(1), 56-59 (2009).